Post-print of the article published on:

Journal of Membrane Science (2021)

Cite this article as:

H.M. Saif, R.M. Huertas, S. Pawlowski, J.G. Crespo, S. Velizarov, Development of highly selective composite polymeric membranes for Li^+/Mg^{2+} separation, *Journal of Membrane Science*, 620 (2021) 118891 https://doi.org/10.1016/j.memsci.2020.118891

Development of highly selective composite polymeric membranes for Li^+/Mg^{2+} separation

H.M. Saif[1], R.M. Huertas[1,2,*], S. Pawlowski[1, *], J.G. Crespo[1], S. Velizarov[1]

[1]LAQV-REQUIMTE, DQ, FCT, Universidade NOVA de Lisboa, 2829-516 Caparica, Portugal

[2]iBET, Instituto de Biologia Experimental e Tecnológica, Apartado 12, 2780-901 Oeiras, Portugal

*Corresponding authors: E-mail: rosa.huertas@ibet.pt (R.M. Huertas), s.pawlowski@fct.unl.pt (S. Pawlowski).

Abstract: To meet the exponentially rising demand for lithium, it becomes vital to develop environmentally friendly processes for its recovery from brines, salt lakes and/or seawater. In this work, novel composite lithium transport selective polymeric membranes were developed to separate lithium and magnesium ions. Hydrogen manganese oxide (HMO) (at weight percentage from 0 to 25 %), polystyrene sulfonate sodium salt (PSS-Na) and lithium triflate ($LiCF_3SO_3$) were added into the sulfonated polyethersulfone (SPES) matrix to prepare composite membranes. The developed

membranes showed high mechanical stability and a homogeneous distribution of HMO. The most promising membrane, containing 20 % (w/w) of HMO, showed an almost 13 times higher Li^+ ionic conductivity (8.28 mS/cm) compared to the control composite membrane (without HMO) and an average ideal selectivity of 11.75 for the Li^+/Mg^{2+} pair. The composite-20% membrane had the lowest intermolecular distance between the polymer chains (according to X-ray diffraction (XRD) analysis), the most flexible structure (lowest T_g) and showed the homogeneous dispersion of HMO (SEM images), which explains its highest Li^+/Mg^{2+} selectivity among the tested membranes. The lithium ion transport performance and separation efficiency were investigated through diffusion dialysis experiments, under different operating conditions. A binary separation factor of 9.10 for Li^+/Mg^{2+} and Li^+ molar flux of 0.026 mol/(m^2.h) was achieved without applying any external potential difference. When an external potential difference of 0.2 V was applied, the binary separation factor of Li^+/Mg^{2+} pair was 5, while the Li^+ molar flux increased almost 5 times. The obtained results provide the basis to design and develop composite lithium transport selective polymeric membranes, thus representing a promising step for future implementation of such membranes to recover lithium from saline streams.

Keywords: Lithium recovery, Composite membranes, Lithium ion sieves (LIS), Sea mining, Diffusion dialysis

1. Introduction

The demand for lithium is rapidly increasing due to the growing lithium-ion battery market which already represents the largest share (~65 %) of the global lithium consumption (57.7 kt in 2019) [1–5]. It is therefore expected that the annual lithium carbonate consumption will reach 350 kt by 2025 [5]. Lithium can be extracted from land reserves (by methods harsh for the environment) and/or from aqueous streams such as brines and seawater, which contain almost 27 Mt of lithium (62 % of the total worldwide lithium resources) [3–9]. The main challenge to selectively recover lithium from such

saline streams is its low concentration and the presence of other cations such as Na^+, K^+ and Mg^{2+} [3–7]. Membrane technologies (pressure or electrochemically driven) offer environmentally friendly separation options, with relatively low energy costs and negligible use of chemicals, compared to conventional evaporation processes, which make them promising options for a sustainable recovery of lithium from saline streams [3–7].

In this work, the focus is on the development of lithium selective composite membranes for Li^+/Mg^{2+} separation, suitable to be used in dialysis [10,11], electrodialysis [12–16] and membrane capacitive deionization [17,18]. These electro-membrane processes were already explored to recover lithium from saline streams, but more selective membranes are needed [5–7]. Hoshino [19] reported the use of ionic superconductor type crystals as a ceramic membrane in a dialysis process for lithium recovery from seawater but, due to a low membrane conductivity, the lithium recovery rate was very slow. Moreover, the mechanical stability of these membranes was limited. Polymeric ion exchange membranes, such as sulfonated polyethersulfone membranes, poly(ethylene-co-vinyl alcohol) membranes and poly(ethylene terephthalate) membranes were also tested, but the exhibited Li^+/Mg^{2+} separation factor was below 1.5 [20,21]. To improve the permeability of monovalent cations and, at the same time, hinder divalent cations transport, Sheng et al. [22] incorporated commercial ZSM-5 zeolite within poly(vinyl alcohol) (PVA) polymer and obtained a Li^+/Mg^{2+} separation factor of 3.7. Afsar et al. [23] coated a sulfonated poly(vinyl alcohol) (SPVA) membrane with a cationic quaternized poly (2, 6-dimethyl-1, 4-phenylene oxide) layer and a Li^+/Mg^{2+} separation factor up to 12.7 was achieved, since the coated cationic layer allowed for cations separation by differences in their charge densities. More recently, the same authors [24] mixed quaternized poly (2, 6-dimethyl-1, 4-phenylene oxide) and amino isophthalic acid (AIPA) to prepare zwitterion membranes, via sol-gel process, which had a Li^+/Mg^{2+} separation factor of 8. Guo et al. [25] developed a metal-organic framework (MOF) on a

threaded sulfonated polymer achieving a very high Li^+/Mg^{2+} binary separation factor of 1815; however, the very brittle nature of the MOF film limits its large scale use.

Zhang et al. [26] prepared a composite cation exchange membrane by dispersing hydrogen manganese oxide (HMO) into a sulfonated polyether ether ketone, and a Li^+/Mg^{2+} separation factor of 3.1 was obtained, while Sharma et al. [27] dispersed magnesium-doped lithium manganese oxide in sulfonated polyether ether ketone, achieving a Li^+/Mg^{2+}selectivity factor of 4.82. The inorganic adsorbents such as $Li_{1.6}Mn_{1.6}O_4$ and $Li_{1.33}Mn_{1.67}O_4$ (LMO compounds) demonstrate a high Li^+ selectivity and an adsorption capacity of up to 40 mg/g [28]. This is attributed to the presence of special lithium transferring channels in the spinel type manganese dioxide frameworks, which act as a lithium ion sieve, because of the existence of cavities in the LMO crystal structure, which size only matches with Li^+ and excludes bigger cations like Na^+, K^+ and Ca^{2+} [29]. Although the crystallographic sizes of Mg^{2+} and Li^+ are similar, Mg^{2+} does not enter into the LMO cavities due to its much higher hydration energy [26,30], thus cation exchange membranes with incorporated LMO derived compounds have been found promising membranes to selectively separate lithium from other cations.

Herein, we report a method to produce chemically, mechanically and thermally stable composite lithium transport selective polymeric membranes by dispersing hydrogen manganese oxide (HMO) into sulfonated polyethersulfone, with the addition of sodium salt of polystyrene sulfonate (PSS-Na) and lithium salt ($LiCF_3SO_3$). The selectivity of the developed membranes was assessed via a comparison of current-voltage curves and by following the transport of ions in diffusion dialysis experiments, performed with and without applying an external potential difference.

2. Materials and Methods

2.1. Materials

Lithium carbonate (Li_2CO_3, Sigma-Aldrich, 99.9 %) and manganese carbonate ($MnCO_3$, Sigma-Aldrich, 99.5 %) were used to prepare the LMO adsorbent. Commercial polyethersulfone (PES) (Ultrason® E6020P), purchased from BASF, was chosen to prepare sulfonated polyethersulfone (SPES). Chlorosulfonic acid (CSA) ($ClSO_3H$, Sigma-Aldrich, 97 %) and sulfuric acid (H_2SO_4, 97 %) were used to promote the sulfonation of the PES backbone. Dimethylformamide (DMF, Sigma-Aldrich, 99.5 %) was used as a solvent. Lithium triflate ($LiCF_3SO_3$, Alfa Aesar, 99.5 %) was used as a bulky anion plasticizer to induce polymer flexibility. Hydrochloric acid (HCl, Sigma-Aldrich, 37 %) was used to protonate the lithium selective adsorbent. Lithium chloride (LiCl, Alfa Aesar, 99.9 %) and magnesium chloride ($MgCl_2$, Sigma-Aldrich, 99 %) were used to prepare the working solutions. Sodium hydroxide (0.01 M NaOH, Sigma-Aldrich, 97 %) standard solution and phenolphthalein (Sigma-Aldrich, 0.5 w% in ethanol : water (1:1)) were used in titration experiments. All reagents were used as received.

2.2. Preparation of composite membranes

Composite membranes were prepared in three steps (Figure 1). The preparation of HMO (step 1) and SPES (step 2) was done in parallel, while in the last third step HMO, PSS-Na and $LiCF_3SO_3$ were incorporated into SPES and the formed membranes were labelled as Composite-X% where X is the weight percentage of HMO to SPES (X = 0, 5, 10, 15, 20, 25 %).

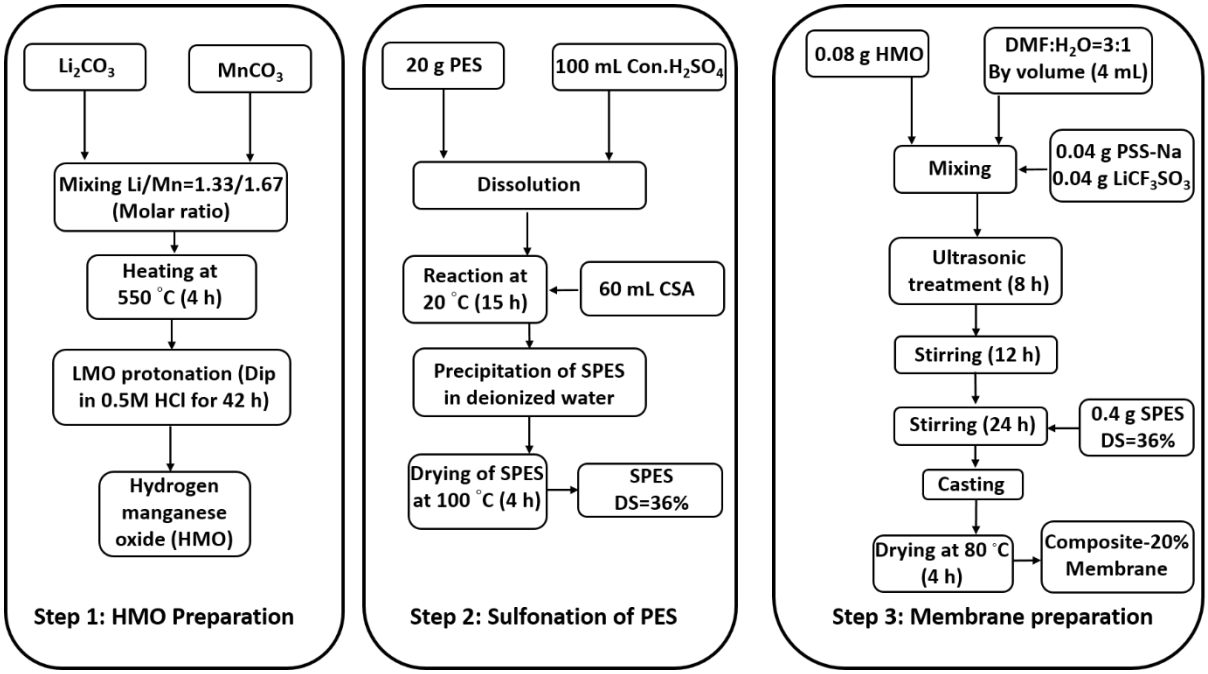

Figure 1. Steps followed in the preparation of composite-20% membrane.

2.2.1. Synthesis of HMO

The solid-state fusion method was used to prepare the lithium manganese oxide LMO ($Li_{1.33}Mn_{1.67}O_4$) powder. Li_2CO_3 and $MnCO_3$ with a molar ratio of Li/Mn = 1.33/1.67 were well mixed in a mortar and the prepared reaction mixture was placed in a ceramic boat and heated in an oven for 4 h at 550 °C under air atmosphere [31,32]. Afterward, Li^+ was extracted from the LMO adsorbent to convert into its protonated form by dissolving 5 g of LMO in HCl solution (0.5 M, 500 mL) stirred for 42 h at room temperature. The resultant mixture was filtered through a 0.4 micron ceramic filter and washed several times with deionized water until achieving a neutral pH. The filter cake was air-dried at 70 °C for 24 h [33].

2.2.2. Sulfonation of PES

Polyethersulfone (PES) was selected as a polymer matrix because of its excellent thermal, mechanical and chemical properties (abundant sulfonate groups and high chemical resistance) and relatively low cost [34]. Chlorosulfonic acid (CSA) was used as a sulfonating agent since it is less expensive and allows for a uniform electrophilic substitution, so there is no need for additional post-treatment, in contrast to the other sulfonating reagents like SO_3 and Oleum [35]. 20 g of PES was dissolved under stirring in 100 mL of concentrated sulfuric acid (97 %) at room temperature to form a homogeneous solution. Subsequently, 60 mL of chlorosulfonic acid (CSA) was added gradually drop wise into the reaction mixture with continuous vigorous stirring at a constant temperature of 20 °C using an ice bath. The sulfonation reaction was time dependent and an optimal 36 % of sulfonation degree (DS) was achieved after 15 h, as analysed by ^{1}H-NMR (Section S2.2. in the Supplementary Information (SI)). Final SPES polymer was obtained by gradual precipitation of the reaction mixture into ice-cold deionized water. The precipitates were recovered by filtration through a 50 mesh screen and washed with de-ionized water until the pH value 7 was achieved. The final product was dried in an oven at 100 °C for 4 h.

2.2.3. Membranes preparation

SPES, with DS = 36 %, and HMO, prepared in the previous steps, were used for membrane fabrication. The degree of sulfonation (DS) of PES is limited to 40 % since above this value SPES starts to dissolve in water. Therefore, the PSS-Na was also introduced to increase the number of sulfonating groups in the membrane structure. Additionally, lithium salt ($LiCF_3SO_3$) was incorporated to increase the flexibility of the final structure of the membrane [36]. Both, PSS-Na and $LiCF_3SO_3$, have poor solubility in pure DMF, thus, to prepare a homogeneous solution for membrane casting, deionized water with DMF in a volume ratio 1:3 was used as a solvent to prepare the films. A pre-defined quantity of HMO (X), 0.04 g PSS-Na and 0.04 g $LiCF_3SO_3$ were dispersed in 4 mL of solvent. The quantities of PSS-Na and $LiCF_3SO_3$ were optimised to grant good mechanical stability to the membranes. The obtained mixtures

were subjected to ultrasonic treatment for 8 h to achieve uniform dispersion of the components. Afterward, the solutions were stirred vigorously for 12 h, 0.4 g of SPES was added and again the mixture was stirred for another 24 h to achieve a homogeneous solution. The formed solution was casted on a glass petri dish and dried at 45 °C for the first 12 h, at 60 °C for the next 12 h and finally at 80 °C for the last 6 h. The synthesized membranes were immersed for 24 h in a 0.1 M HCl solution to leach out the remaining Li^+ and Na^+ ions. The amount of both ions in HCl solution was the same after 24 and 48 h, thus there was no additional leaching of lithium and sodium after 24 h. Finally, the membranes were thoroughly washed with deionized water several times and dried in an oven at 80 °C for 4 h. The thickness of the prepared membranes was 100 μm ± 5 μm.

2.3. Characterisation methods

The lithium selective adsorbent (HMO) was characterised via XRD to confirm its spinal type structure and by FT-IR to identify the existing main bonds. The thermal stability, degree of sulfonation and chemical structure of sulfonated polyethersulfone (SPES) polymers were examined by TGA, titration and ^{1}H-NMR, and FT-IR, respectively. The experimental details and results obtained with regard to the characterisation of HMO and SPES are presented in the Supplementary Information. The hydrophilicity, chemical, thermal, mechanical, structural and morphological properties of the composite membranes were studied using contact angle measurement, water uptake, FT-IR, TGA and DSC, tensile testing assays, XRD and SEM techniques, respectively. The ideal selectivities and Li^+/Mg^{2+} binary separation factors of the composite membranes were obtained through experimental performance in a dedicated diffusion cell. The composite membrane offering the most selective lithium transport was tested twice, as pristine and after being used for 10 h in diffusion experiments.

2.3.1. Physical properties analysis

2.3.1.1. Water content

A piece of a dry membrane with dimension 1×1 cm^2 was immersed in deionized water for 24 h and weighed after removing excessive water on both surfaces with filter paper. The wet membrane was placed in the vacuum oven at 60 °C for 24 h and weighed again. The percentage of water content (WC) was determined as [37]:

$$WC\ (\%) = \frac{W_{wet} - W_{dry}}{W_{dry}} \times 100 \qquad (\text{eq. } 1)$$

2.3.1.2. Membrane hydrophilicity

The hydrophilicity of the synthesised membranes was examined by contact angle measurements using a goniometer (Dyne technology, UK) coupled with a KSV CAM2008 equipment. Before analysis, each membrane sample with a dimension 2×2 cm^2 was washed with deionized water and dried overnight, at a room temperature, in a desiccator. A sessile drop of deionized water (10-12 µL) was placed on the membrane surface. Each measurement was attained with 20 frames with a frame interval of 100 ms. For each membrane, the average value of the contact angle was calculated from the measurements taken at three different random places.

2.3.2. Structural and morphological properties

2.3.2.1. Fourier transform infrared spectroscopy (FT-IR)

Fourier Transform Infrared Spectra (FT-IR) using attenuated total reflectance (ATR) mode was used to determine the chemical structure of HMO (Figure S1, SI), SPES polymers (Figure S6, SI) and the prepared composite membranes (Figure S8, SI). The spectrum of the best composite membrane was recorded at both sides of the membrane, before and after used (10 h in diffusion dialysis experiments), to observe any structural modification which may have occurred during the experiments. The

equipment employed was a Bruker Spectrometer IFS 66/S FT-IR instrument (USA) equipped by H-ATR with ZnSe crystal. Before analysing, samples were dried overnight in a desiccator at room temperature. Samples were taken from random positions of the membrane to check the homogeneity of the structure. The normalized spectra were recorded in the range of wave numbers from 4000 to 500 cm^{-1} during 20 scans with a 2 cm^{-1} resolution.

2.3.2.2. X-ray diffraction (XRD)

The morphology of the synthesised composite membranes and the lithium selective adsorbent was studied by x-ray diffraction (XRD) technique. Diffraction patterns were documented on a MiniflexII diffractometer (Rigaku, Japan) using monochromatic Cu Kα radiation (λ = 1.542 Å, 30 kV, 15 mA). The average distance (d-spacing, Å) between the polymer chains or the spacing between the crystalline phases (d, Å) were calculated using the Bragg's equation:

$$n\lambda = 2d \cdot Sin\theta_{max} \qquad (\text{eq. } 2)$$

where λ = 1.542 Å and 'n' is an integer that represents the order of reflection [38].

2.3.2.3. Scanning Electron Microscopy with Energy Dispersive X-Ray Spectroscopy (SEM-EDS)

The morphology and surface composition of the composite membranes were analysed via the scanning electron microscopy (SEM) technique using a Carl Zeiss AURIGA Cross Beam FIB-SEM workstation. The presence of manganese atom in the composite membranes was identified semi-quantitatively by an energy dispersive spectroscopy using an X-ray detector (Oxford, model INCA 150). Samples were prepared by cryogenic fracture under liquid nitrogen and made electrically conductive using a Sputter Quorum with 15 nm thick Au/Pd film.

2.3.3. Thermal properties analysis

2.3.3.1. Thermogravimetric analysis (TGA)

A TGA Q-50 analyzer (TA Instruments, USA) was employed to determine the degradation temperature and inorganic content using a ramp of 10 ˚C/min, in the temperature range of 25 to 600 ˚C under a nitrogen atmosphere with a flow rate of 40 mL/min. The approximate sample weight was 5 mg placed into an aluminium sample pan. The inorganic content and thermal behaviour of the membranes were analysed under inert atmosphere at 600 ˚C from TGA curves.

2.3.3.2. Differential scanning calorimetry (DSC)

The glass transition temperature (T_g) of the synthesised composite membranes was calculated from differential scanning calorimetry (DSC) data. The DSC analysis was performed on a TA DSC Q-200 equipment (TA Instruments, USA). The temperature range of 0–300 ˚C was set in the DSC analysis, based on the degradation pattern obtained from TGA study. Prior to the analysis, the samples were dried in a desiccator and the approximate weight of each sample was 8 mg. The analysis was carried out under nitrogen atmosphere with a flow rate of 40 mL/min and a heating rate of 20 °C /min. Samples were subjected to three rapid heating-cooling cycles: heating for deleting the thermal history, cooling and a final heating. The inflection point of the variation in the specific heat was taken as T_g.

2.3.4. Mechanical properties analysis

Mechanical properties of the composite membranes were examined by tensile testing assays measured on texture analyser equipment (TAXT plus, Stable Micro Systems, England) using the load cell of 5 kg. The tensile strength (TS) and Young's modulus were determined by using rectangular membrane strips (10.5 mm × 25 mm). The samples were hanged between the grips of the texture analyser and the crosshead speed was set at 0.5 mm/s. Two strips of each membrane were analysed and the average value was calculated.

2.3.5. Evaluation of lithium transport

The performance of the prepared composite membranes was compared in terms of their ideal selectivity and binary separation factor. Experiments were performed using a cylindrical diffusion cell with 2 compartments of 186 mL capacity each (Figure 2). The active membrane area in the cell was 11.34 cm^2. Copper rods were used as electrodes.

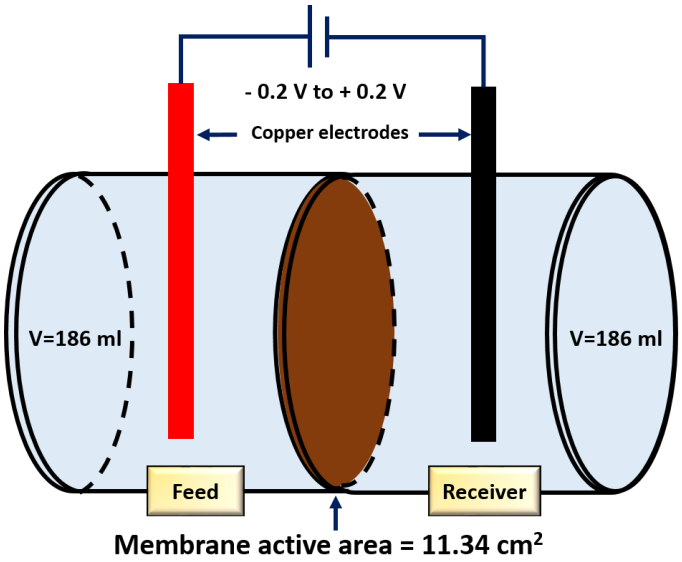

Figure 2. A schematic configuration of the diffusion cell used in the experiments.

2.3.5.1. Ideal selectivity

The ideal selectivity values for Li^+/Mg^{2+} were evaluated via current-voltage curves obtained through linear sweep voltammetry (LSV), by Vertex 5A potentiostat (Ivium Technologies). A scan rate of 200 mV/s, at a step of 1 mV for the potential difference range between - 0.2 V and + 0.2 V were used as LSV operating conditions. In these experiments, the feed and the receiver side of the diffusion cell contained the same salt solution (0.1 M LiCl or 0.1 M $MgCl_2$). The membranes under study were equilibrated for one hour in the respective salt solution before measuring the current-voltage (I-V) curves. The slope of the linear part of the I-V curve gives the conductance value of the membrane immersed in a given salt solution. The ratio of slops of I-V curves obtained for different salt solutions gives the ideal selectivity of counter-ions (in the present case Li^+/Mg^{2+}) pair.

2.3.5.2. Binary separation factor

The binary separation factor between lithium and magnesium was defined as a ratio of their degrees of recovery in the receiver:

$$Binary\ separation\ factor = \frac{[Li^+]^R_{t=t} \Big/ [Li^+]^F_{t=0}}{[Mg^{2+}]^R_{t=t} \Big/ [Mg^{2+}]^F_{t=0}} \quad \text{(eq. 3)}$$

where $[Li^+]^R_{t=t}$, $[Mg^{2+}]^R_{t=t}$ are molar ionic concentrations of lithium and magnesium in the receiver at time 't' (herein after 5 h), while $[Li^+]^F_{t=0}$, $[Mg^{2+}]^F_{t=0}$ are the initial molar ionic concentration of lithium and magnesium in the feed, respectively. The binary separation factor was examined by using equimolar solutions of 0.25 M of LiCl and 0.25 M $MgCl_2$ in the feed compartment and deionized water in the receiver. These experiments were conducted under two different diffusion dialysis operating conditions: without applying potential difference and with an applied potential difference of + 0.2 volts across the investigated membrane. The ionic compositions of the feed and the receiver were analysed by inductively coupled plasma atomic emission spectroscopy (ICP-AES). Samples (2 mL each) were taken after 5 h from the two compartments of the diffusion cell.

3. Results and Discussion

3.1. Membrane characterisation

3.1.1. Water uptake and surface hydrophilicity

In sulfonated polymers, the water uptake increases with the sulfonation degree (DS). For pure PES there is a negligible water uptake, while for the composite-0% membrane, with DS 36 %, it became significant (Figure 3). The molecular structure of SPES consists of a hydrophobic backbone and hydrophilic sulfonic acid groups. The hydrophilic part of the structure is mainly responsible for water uptake in polymers. Within the composite membranes, the increase of HMO content also leads to an increase in the water uptake, since HMO has a hydrophilic nature [39,40].

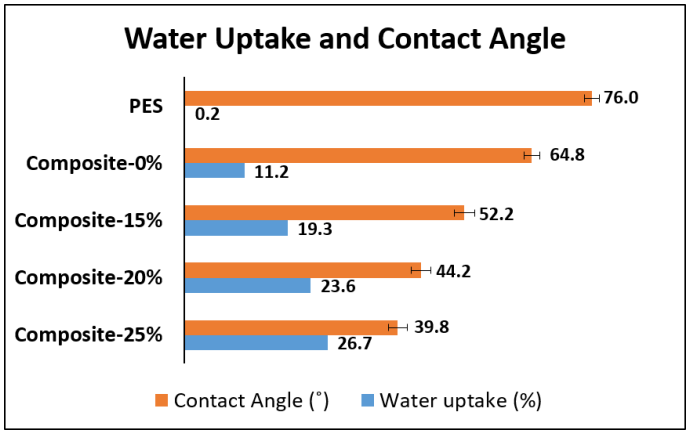

Figure 3. Comparison of water uptake and contact angle of pure polyethersulfone membrane and composite membranes.

The prepared membranes also showed the expected trend in contact angle measurements. PES is mildly hydrophilic, with a contact angle value of 76 °, while an increase in DS leads to a slight decrease of the contact angle to around 65 ° for composite-0% membrane due to an increase in the hydrophilic part of its structure. For the composite-15%, 20% and 25% membranes, the contact angle further decreased due to the increasing content of the hydrophilic HMO filler from 15 to 25 wt% in the polymer matrix.

3.1.2. FT-IR analysis

The chemical compositions of the prepared composite-0%, 15%, 20% and 25% membranes were confirmed by analysing the respective FT-IR spectra (Figure S8, SI). As expected, the FT-IR spectrum for composite-0% membrane exhibited the same peaks as the SPES with DS = 36 % (Section S2.3., Figure S6, SI) which was used to prepare this membrane. The FT-IR spectra of the composite-15%, 20% and 25% membranes, which have a HMO powder and a lithium triflate salt in their structure, present a peak at 1650 cm^{-1} (hydroxyl (-OH)) of water adsorbed due to the presence of the hydrophilic HMO powder [41]). Also, the characteristic broad band at around 3450 cm^{-1}, associated with the vibrational stretching of –OH groups, increased its intensity when HMO was added. The presence of the HMO

adsorbent was also confirmed by the presence of a new peak at 639 cm^{-1} which is associated with Mn-O bond stretching [42]. Compared to the SPES polymer (Section S2.3, Figure S6, SI), in composite membranes the band intensity at around 1024 cm^{-1} increased due to the overlapping of the SO_3^- groups related spectrum, provided by the addition of a $CF_3SO_3^-$ anion and aromatic SO_3H groups of sulfonated polymer matrix. These peaks confirm not only the presence of $LiCF_3SO_3$, but also the addition of "extra" SO_3^- groups provided by this salt.

Figure 4 shows the FT-IR spectra for the most promising membrane (composite-20%) before and after being tested in 10 h of diffusion dialysis experiments. The results, which are complementary with the XRD analysis, are discussed in more detail in the following section, but shortly, it is possible to see that all the characteristic peaks remained unaffected after the tests, therefore the FT-IR analysis confirms that the chemical structure of the composite membrane is stable under the applied operating conditions.

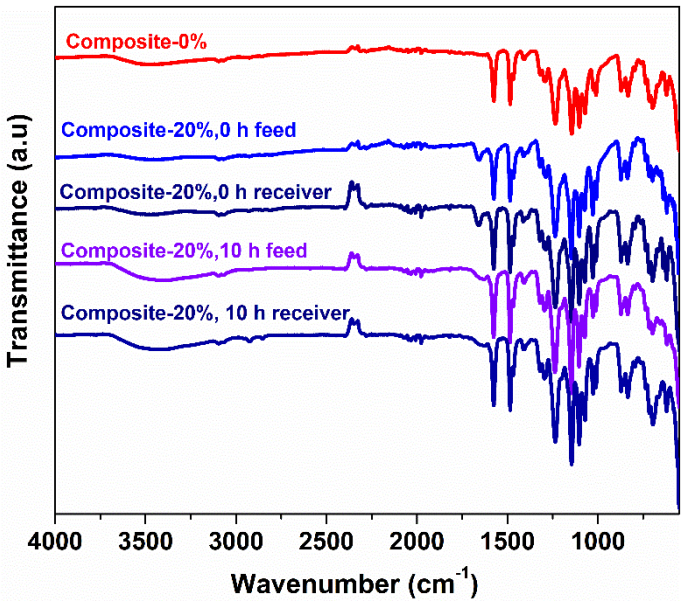

Figure 4. Vertically shifted FT-IR spectra of the composite-20% membrane before used (pristine) and after diffusion tests (10 h), compared to pristine composite-0% membranes.

3.1.3. X-ray diffraction (XRD) analysis

X-ray diffraction patterns were used to determine the presence or absence of the crystallinity in the prepared membranes. Figures 5a and 5b show the diffractograms of composite-15%, 20% and 25% pristine membranes and composite-20% membrane before (pristine) and after being used, respectively.

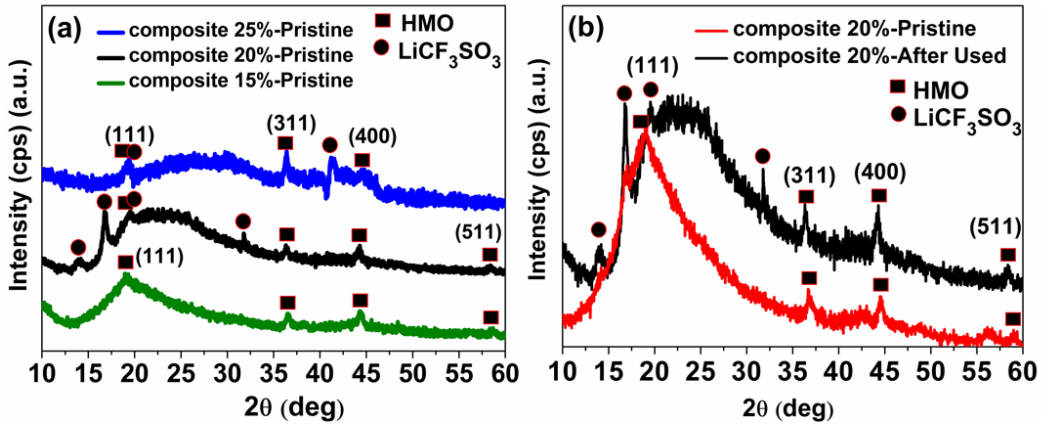

Figure.5 Vertically shifted XRD normalized diffractograms of **(a)** composite-15%, composite-20% and composite-25% pristine membranes and **(b)** composite-20% pristine membrane (before use) and after 10 h used. (The Intermolecular average distance was calculated using Braggs' law, as summarized in Table S3, SI).

The diffractograms of pristine composite-15%, 20% and 25% membranes showed a typical amorphous halo maximum along with the crystalline diffraction peaks for HMO and lithium salt ($LiCF_3SO_3$) (Figure 5a). The peaks at around 2θ = 14°, 16.27°, 19.5°, 22.24°, 31.98°, 39.65° and 48.35 degrees could be attributed to the presence of lithium salt [43,44]. For the pristine composite-15%, 20% and 25% membranes, the amorphous halo appeared centred at 2θ = 19°, 22.7° and 28°, which corresponds to an intermolecular average distance of 4.5 Å, 3.1 Å, and 3.8 Å, respectively. This indicates that each membrane possessed the different polymer chains packing. Moreover, these values follow the same trend observed for glass transition temperature (T_g) (analysed and discussed in section 3.1.5.) and they

are also in a good agreement with the Li^+ ion ideal selectivity results (Table 2). As can be seen, the lowest average intermolecular distance between the polymer chains was observed for the pristine composite-20% membrane, which is the membrane with the highest Li^+ ideal selectivity. The amorphous halo for the used composite-20% membrane was displaced and centred at 2θ = 19.2° which is equivalent to an average distance of 4.5 Å (Figure 5b). The increased average distance between polymer chains, after use, depicts a loose polymer chains packing within the membrane structure, probably due to the swelling of polymer matrix which is directly related to the hydrophilicity of the sulfonated parts of the polymer [45]. Moreover, crystalline peaks with low intensity were detected, which have the same 2θ values as observed for HMO powder and $LiCF_3SO_3$ salt. The appearance of these peaks also indicates that those components maintained their crystalline structure inside the composite membrane which allowed for the selective lithium transport through the membrane [46].

3.1.4. Morphology

The comparison of surface and cross-section morphology of the prepared composite membranes (0%, 15%, 20% and 25%) is shown in Figure S9 in the Supplementary Information. SEM images revealed that these composite membranes have a dense structure and an increasing content of HMO from 0 to 25 wt%, which promotes additional roughness in the structure of the composite membrane. Figure S9 also shows that up to 20 wt% the HMO is homogeneously distributed in the membrane matrix. However, with the further increase (more than 20 wt%), HMO starts to aggregate, resulting in formation of cracks inside the membrane structure (Figure S9 (d and g), SI), which additionally explains why the composite-20% membrane (with the highest uniformly distributed HMO content) showed the highest lithium transport among all the prepared membranes.

The composite-20% membrane was analysed before and after used in diffusion experiments to check for any significant changes in the morphology (Figure 6 (a-d)) and in Mn element distribution (Figure 6 (e-f)).

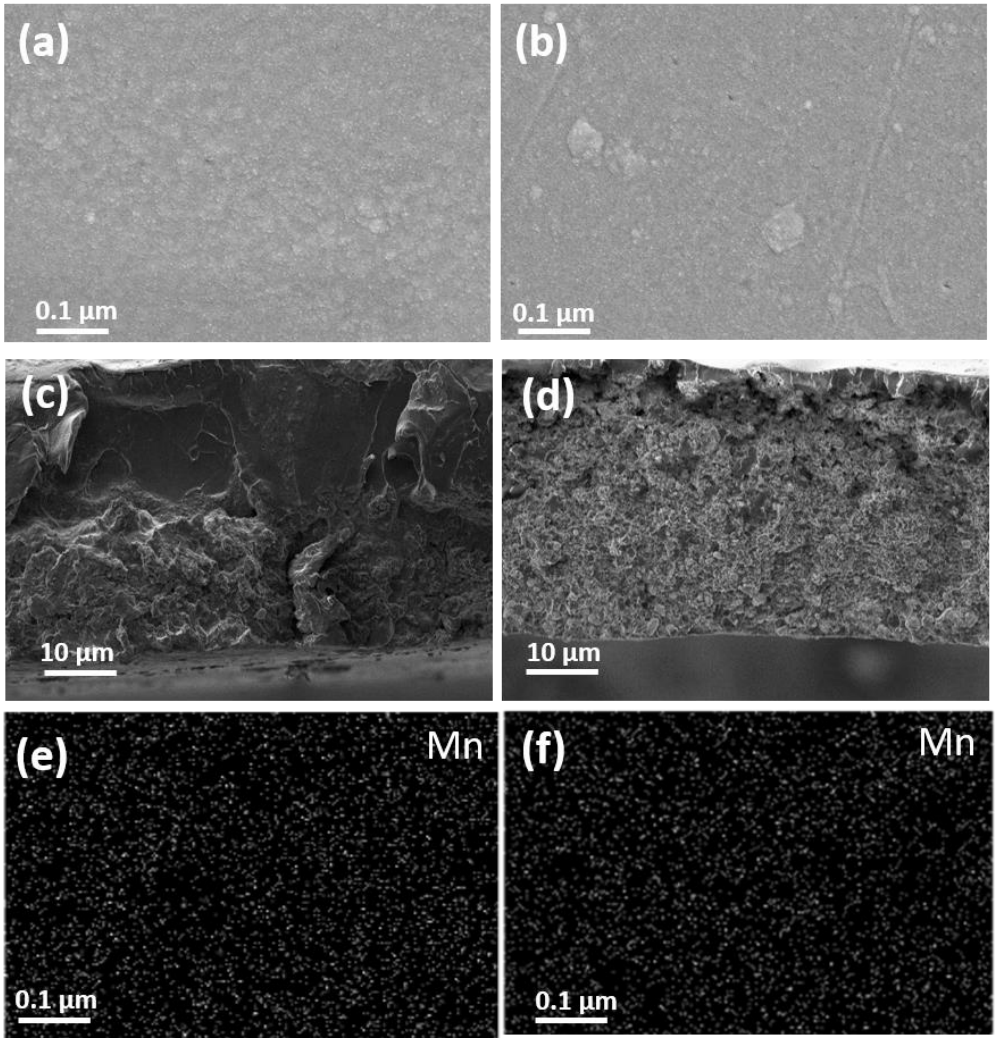

Figure 6. SEM images of **(a)** composite-20% surface before use, **(b)** composite-20% surface after use, **(c)** composite-20% cross section before use, **(d)** composite-20% cross section after use, **(e)** EDX map for Mn atom on (a), **(f)** EDX map for Mn atom on (b).

The cross-section images (Figure 6c-d) show that the composite-20% membrane exhibited a good compatibility between inorganic adsorbent and polymeric matrix, leading to a homogeneous and a uniform dispersion that was maintained after the membrane usage in diffusion experiments. The homogeneous distribution of the manganese (Mn) atom was also confirmed by EDX maps for

composite-20% membrane (Figure 6e-f). Moreover, a very small difference between the atomic composition of the pristine and used composite-20% membrane (22.95 ± 4.86 % vs. 21.00 ± 3.25 % for Mn, respectively) confirmed the stability of the inorganic component in the polymeric matrix, as expected based on FT-IR results (Figure 4 and Section 3.1.2.). Thus, no drastic visible changes in the surface morphology of the composite-20% membrane were observed after the membrane had been used.

3.1.5. Thermal properties

Thermal properties of the composite membranes (0%, 15%, 20% and 25%) obtained by TGA and DSC are shown in Figure 7a and 7b, respectively.

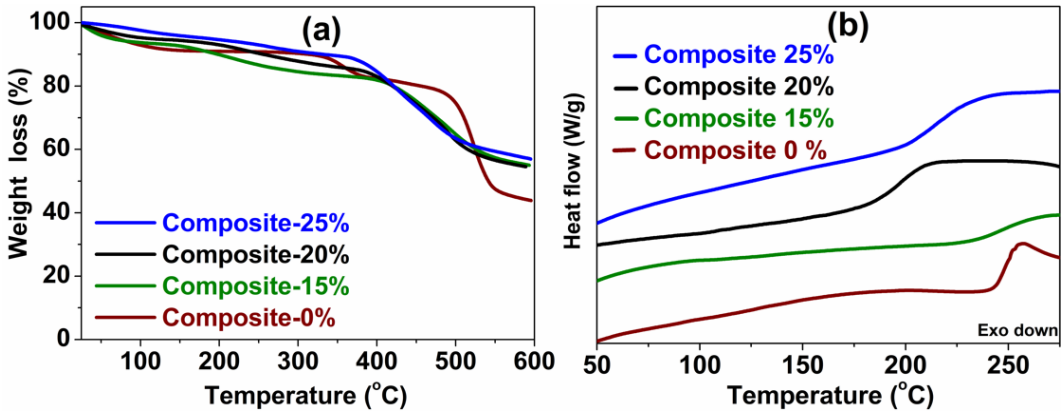

Figure 7. TGA **(a)** and vertically shifted DSC **(b)** curves of composite-0%, 15%, 20%, and 25% membranes.

Composite-0%, 15% and 20% membranes presented three weight loss steps (Figure 7a). The first weight loss can be attributed to the removal of strongly adsorbed water molecules within the polymeric matrix (water adsorbed by the interaction of hydrophilic –OH groups with $–SO_3^-$ groups [26]). The second weight loss is due to the removal of pendant groups (low bond energy) in the polymer and the third weight loss is due to the thermal degradation of the polymeric backbone. The composite-25% membrane, because of its high HMO content, presented only two main degradation steps which are representative for the thermal behaviour of HMO (Figure S3, SI). By comparing the

second weight loss temperature recorded for composite-0%, 15% and 20% membranes (Table S4, SI), we can observe a decreasing trend in temperature from 330 °C for composite-0% membrane to 194 °C for composite-20%. This effect is most probably caused by the addition of the HMO adsorbent, which has a relatively low thermal stability (Td onset = 200 °C, Table S4, SI). Therefore, an inverse trend was observed between the thermal stability and the increase of HMO content in the polymeric matrix. This can also explain the overlap between second and third weight loss in the composite-25%. In the third weight loss step, the temperature was above 400 °C for all the composite membranes (Table S4, SI), demonstrating that the presence of the HMO adsorbent does not reduce the thermal stability of the composite membranes.

The highest residue at 600 °C was measured for HMO powder, as expected, due to its inorganic nature and, consequently, a 14 %, 16 % and 18 % rise in residue was observed for composite-15%, 20% and 25% membranes, respectively, compared to the composite-0% membrane (Table S4, SI). Thus, it confirms the incorporation of HMO into the polymer matrix.

The DSC curves of composite-0%, -15%, -20% and -25% membranes (Figure 7b) show a change in the heat capacity associated with the glass transition temperature (T_g), attributed to the polymeric segments in the composite membranes. The T_g value reported for pure PES is 230 °C [47], and for the composite-0% membrane, it increased to 251 °C (Table S4, SI). This could be attributed to the introduction of sulfonic acid groups into the polymer chains, which caused an increase of intermolecular interactions between the polymer chains, resulting in a higher glass transition temperature. T_g values obtained for composite 15%, 20% and 25% membranes were lower compared to the composite-0% and ranged between 249 °C and 197 °C (Table S4, SI). However, there was no clear trend observed between the HMO content and T_g. Instead, T_g first decreased for composite-15% and 20% and then slightly increased for composite-25% membrane. The addition of HMO and lithium

triflate salt can lead to decrease of the T_g values because the presence of an inorganic filler may constrain the intermolecular interaction between the polymer chains [35,48,49] and $LiCF_3SO_3$ salt acts as a $–SO_3$ group-provider and plasticizer, thus it increase the flexibility of the structure [35,48,49]. Therefore, the behaviour observed for the composite-15% and 20% and 25% membranes can be explained by the optimal HMO content being equal to 20%. Above 20%, the T_g increased most probably because the high HMO content could lead to the aggregation of polar groups on HMO through hydrogen interactions [26].

3.1.6. Mechanical properties

The tensile strength (TS) and Young's modulus values of the composite membranes were calculated from the stress–strain diagram (Figure S10, SI), summarized in Table 1.

Table 1. Tensile strength (TS), and Young's modulus of the composite membranes

Membranes	Tensile strength (MPa)	Young modulus (MPa)
Composite-0%	43.7	803
Composite-15%	37.6	275
Composte-20%	32.7	269
Composite-25%	35.5	289

In general, the tensile strength (TS) and Young's modulus decreased with the addition of HMO content, except for composite-25% membrane. The decrease of the mechanical strength of the composite-15% and -20% membranes, in comparison to the control composite-0% membrane, is associated with the interactions between the hydrophobic part of the polymer (backbone of polymer) and the hydrophilic inorganic filler. Moreover, the insoluble HMO content may hinder the interaction between the polymer chains producing changes or structural discontinuities in highly packed SPES polymeric structure [50,51]. However, for HMO concentrations above 20 wt%, the HMO starts to aggregate and its contact area with the polymer decreases, which favours the interaction between the polymer

chains and increases the mechanical strength [26]. In any case, all the prepared membranes are mechanically stronger than the HMO based polymeric lithium selective membranes reported so far in the literature (TS = 24.7 MPa [26], TS = 5.38 MPa [27]).

3.2. Membrane ion transport performance and lithium selectivity

3.2.1. Ideal selectivity

The I-V curves of the prepared membranes are presented in Figure S11 (a) and (b) in the Supplementary Information, while the corresponding ideal selectivities, calculated from ion conductivity data (Figure 8), are shown in Table 2.

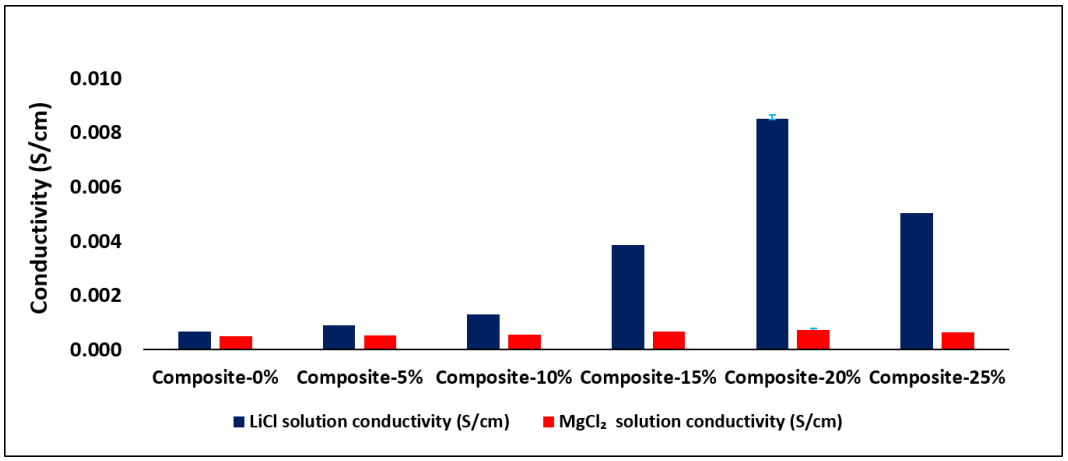

Figure 8. LiCl and $MgCl_2$ solutions conductivities for composite membranes.

Table 2. Li^+ ion ideal selectivity of the composite membranes.

Membranes	Comp-0%	Comp-5%	Comp-10%	Comp-15%	Comp-20%	Comp-25%
Li^+/Mg^{2+}	1.34	1.67	2.39	5.77	11.75 ± 0.55	7.89

The composite-0% membrane showed almost the same conductivity values for lithium and magnesium ion (Figure 8). The slightly lower magnesium conductivity in composite-0% membrane could be due to the higher binding affinity of Mg^{2+} ions compared to Li^+ ions with sulfonic groups of SPES, which may hinder their transport [21]. The incorporation of HMO changed this effect. For

example, merging just 5 % w/w of HMO into the composite membrane increased twice the Li^+ ion conductivity of that membrane, while the Mg^{2+} conductivity remained almost the same. Likewise, the Li^+ ion conductivity continuously increased with the increase in HMO content from 5 % w/w to 20 % w/w and a Li^+/Mg^{2+} ideal selectivity close to 12 was achieved (Table 2), which is a value almost 4 times higher than previously achieved by Zhang et al. [26] and 3 times higher compared to the value reported by Sharma et al. [27]. The sharp increase of Li^+ conductivity with increasing HMO content can be explained by the HMO structure which only allows the free insertion of Li^+ through its 8a-16d-8a interspaces and the synergistic effect of sulfonating groups of the polymer, which have different binding affinity with different cations such as Li^+ = 1.0, Na^+ = 1.98, K^+ = 2.9 and Mg^{2+} = 3.18 (all these values are normalized to Li^+) [21,26]. However, the further increase in HMO content to 25 % w/w lead to the reduction of Li^+ ion conductivity, which is in accordance to the SEM image (Figure S9 d and h) where cracks in surface of the membrane and the aggregation of HMO adsorbent can be seen. The best Li^+ ideal selectivity, obtained for composite-20% membrane, could be also explained by the best flexibility (lowest T_g , section 3.1.5.), the best equilibrium between packing constraints, rigidity and interactions with favourable functional groups ($-SO_3^-$) and the lowest polymer chains packing in the amorphous polymeric phase observed for the pristine composite-20% membrane (XRD, section 3.1.3.).

3.2.2. Binary separation factor and cationic flux

Figures 9a and 9b show the data related to lithium and magnesium molar ionic fluxes and their binary separation factor by composite-20% membrane.

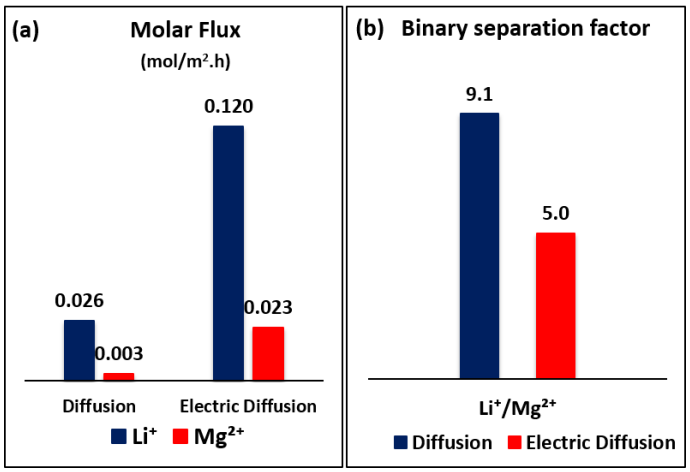

Figure 9. (a) Li^+ and Mg^{2+} ion fluxes in diffusion and electric diffusion experiments, (b) Binary separation factor of Li^+/Mg^{2+} pair by composite-20% membrane.

For diffusion dialysis, the binary separation factor was 9.1 and the lithium molar flux was 0.026 mol/(m^2.h). When an external potential difference of 0.2 V was applied, the binary separation factor decreased to 5, but the Li^+ molar flux increased almost 5 times (0.12 mol/(m^2.h)). In both cases, a lower Mg^{2+} flux could be due to its bigger hydrated size, lower diffusion coefficient and higher binding affinity to sulfonic groups compared to that of Li^+ [25]. When the external potential difference was applied, the external force and the selective nature of the membrane boosted the Li^+ flux but the flux of Mg^{2+} also increased significantly, possibly because Mg^{2+} is doubly charged so it experiences the double of the electric force (compared to Li^+), which could increase its transport by migration. Table S5 (SI) summarises the lithium Ion flux and binary separation factor of different membranes at different operating conditions reported in the literature.

Based on the conditions used, and on the obtained results, this work showed a clear progress in the preparation of composite cation exchange membranes and demonstrated how to develop mechanically stable membranes showing an improved separation between lithium and magnesium at a relatively low applied external potential difference. Given the promising potential, their use in

membrane capacitive deionization and/or electrodialysis processes for selective lithium recovery could be foreseen.

4. Conclusions

- Composite lithium transport selective polymeric membranes were developed by merging hydrogen manganese oxide (HMO) into mixture of sulfonated polyethersulfone (SPES), sodium salt of polystyrene sulfonate (PSS-Na) and lithium triflate ($LiCF_3SO_3$).
- The presence of HMO in the membrane not only improved its lithium selectivity, but also increased its hydrophilicity, which led to an increase in ionic fluxes compared to those obtained with the membrane without HMO (composite-0%).
- The highest Li^+/Mg^{2+} ideal selectivity of 11.75 was achieved by the composite membrane containing 20 % (w/w) of HMO.
- In diffusion dialysis, a Li^+/Mg^{2+} binary separation factor of 9.1 was achieved at a Li^+ flux of 0.026 mol/(m^2.h). In electro-diffusion dialysis, when a potential difference of + 0.2 V was applied, the transport performance was improved in terms of lithium flux (0.11 mol/(m^2.h)), while still maintaining a relatively high Li^+/Mg^{2+} binary separation factor of 5.0.
- 20 % (w/w) content of HMO lead to formation of a composite membrane with the lowest intermolecular distance between the polymer chains, the most flexible structure (lowest Tg) and a still uniform dispersion of HMO among the tested membranes, which explains its best performance in term of the lithium separation and transport.
- The performed analyses proved that the prepared membranes are chemically and mechanically stable and adequate for the use at large scale.

The use of lithium selective adsorbents with high adsorption capacity and polymers possessing high IEC could further improve the membrane performance. Overall, this study provides a strong base for the development of highly lithium selective membranes.

Acknowledgments

This project has received funding from the European Union's Horizon 2020 research and innovation programme under grant agreement No 869467 (SEArcularMINE). This work was supported by the Associate Laboratory for Green Chemistry- LAQV, which is financed by Portuguese national funds from FCT/MCTES (UID/QUI/50006/2019). This work was also supported by "*Programa Operacional Regional de Lisboa, na componente FEDER*" and "*Fundação para a Ciência e Tecnologia*, I.P." through research project PTDC/EQU-EPQ/29579/2017. S. Pawlowski acknowledges *Fundação para a Ciência e Tecnologia*, I.P. for his contracts CEECIND/01617/2017 and CEECIND/00340/2018. iNOVA4Health – UIDB/Multi/04462/2020, a program financially supported by Fundação para a Ciência e Tecnologia is acknowledged. Funding from INTERFACE Programme, through the Innovation, Technology and Circular Economy Fund (FITEC), is also gratefully acknowledged. The authors acknowledge Professor Vítor D. Alves, from Instituto Superior de Agronomia, Universidade de Lisboa, for the support to analysing mechanical properties.

References

[1] P.K. Choubey, K.S. Chung, M. seuk Kim, J. chun Lee, R.R. Srivastava, Advance review on the exploitation of the prominent energy-storage element Lithium. Part II: From sea water and spent lithium ion batteries (LIBs), Miner. Eng. 110 (2017) 104–121. https://doi.org/10.1016/j.mineng.2017.04.008.

[2] M.J. Park, G.M. Nisola, E.L. Vivas, L.A. Limjuco, C.P. Lawagon, J.G. Seo, H. Kim, H.K. Shon, W.J. Chung, Mixed matrix nanofiber as a flow-through membrane adsorber for continuous Li+ recovery from seawater, J. Membr. Sci. 510 (2016) 141–154. https://doi.org/10.1016/j.memsci.2016.02.062.

[3] P. Xu, J. Hong, X. Qian, Z. Xu, H. Xia, X. Tao, Z. Xu, Q.Q. Ni, Materials for lithium recovery from salt lake brine, J. Mater. Sci. (2020). https://doi.org/10.1007/s10853-020-05019-1.

[4] Y. Sun, Q. Wang, Y. Wang, R. Yun, X. Xiang, Recent advances in magnesium / lithium separation and lithium extraction technologies from salt lake brine, Sep. Purif. Technol. (2020) 117807. https://doi.org/10.1016/j.seppur.2020.117807.

[5] C. Tang, M.L. Bruening, Ion separations with membranes, J. Polym. Sci. (2020) 1–26. https://doi.org/10.1002/pol.20200500.

[6] Y. Zhao, M. Wu, P. Shen, C. Uytterhoeven, N. Mamrol, J. Shen, C. Gao, B. Van der Bruggen, Composite anti-scaling membrane made of interpenetrating networks of nanofibers for selective separation of lithium, J. Membr. Sci. 618 (2021). https://doi.org/10.1016/j.memsci.2020.118668.

[7] Y. Zhang, L. Wang, W. Sun, Y. Hu, H. Tang, Membrane technologies for Li+/Mg2+ separation from salt-lake brines and seawater: A comprehensive review, J. Ind. Eng. Chem. 81 (2020) 7–23. https://doi.org/10.1016/j.jiec.2019.09.002.

[8] A. Razmjou, M. Asadnia, E. Hosseini, A. Habibnejad Korayem, V. Chen, Design principles of ion selective nanostructured membranes for the extraction of lithium ions, Nat. Commun. 10 (2019). https://doi.org/10.1038/s41467-019-13648-7.

[9] H. Vikström, S. Davidsson, M. Höök, Lithium availability and future production outlooks, Appl. Energy. 110 (2013) 252–266. https://doi.org/10.1016/j.apenergy.2013.04.005.

[10] T. Ounissi, L. Dammak, C. Larchet, J.F. Fauvarque, E. Selmane Bel Hadj Hmida, Novel lithium selective composite membranes: synthesis, characterization and validation tests in dialysis, J. Mater. Sci. 55 (2020) 16111–16128. https://doi.org/10.1007/s10853-020-05147-8.

[11] K. Smolinska, M. Bryjak, J. Wolska, W. Kujawski, pH-sensitive membranes for lithium separation, Mater. Chem. Phys. 148 (2014) 548–553. https://doi.org/10.1016/j.matchemphys.2014.08.003.

[12] J. Ying, M. Luo, Y. Jin, J. Yu, Selective separation of lithium from high Mg/Li ratio brine using single-stage and multi-stage selective electrodialysis processes, Desalination. 492 (2020) 114621. https://doi.org/10.1016/j.desal.2020.114621.

[13] Q.B. Chen, Z.Y. Ji, J. Liu, Y.Y. Zhao, S.Z. Wang, J.S. Yuan, Development of recovering lithium from brines by selective-electrodialysis: Effect of coexisting cations on the migration of lithium, J. Membr. Sci. 548 (2018) 408–420. https://doi.org/10.1016/j.memsci.2017.11.040.

[14] P.Y. Ji, Z.Y. Ji, Q.B. Chen, J. Liu, Y.Y. Zhao, S.Z. Wang, F. Li, J.S. Yuan, Effect of coexisting ions on recovering lithium from high Mg2+/Li+ ratio brines by selective-electrodialysis, Sep. Purif. Technol. 207 (2018) 1–11. https://doi.org/10.1016/j.seppur.2018.06.012.

[15] Z.Y Ji, Q.B. Chen, J.S. Yuan, J. Liu, Y.Y. Zhao, W.X Feng, Preliminary study on recovering lithium from high Mg2+/Li+ ratio brines by electrodialysis, Sep. Purif. Technol. 172 (2017) 168–177. https://doi.org/10.1016/j.seppur.2016.08.006.

[16] X.Y. Nie, S.Y. Sun, Z. Sun, X. Song, J.G. Yu, Ion-fractionation of lithium ions from magnesium ions by electrodialysis using monovalent selective ion-exchange membranes, Desalination. 403 (2017) 128–135. https://doi.org/10.1016/j.desal.2016.05.010.

[17] W. Shi, X. Liu, C. Ye, X. Cao, C. Gao, J. Shen, Efficient lithium extraction by membrane capacitive deionization incorporated with monovalent selective cation exchange membrane, Sep. Purif. Technol. 210 (2019) 885–890. https://doi.org/10.1016/j.seppur.2018.09.006.

[18] S. Pawlowski, R.M. Huertas, C.F. Galinha, J.G. Crespo, S. Velizarov, On operation of reverse electrodialysis (RED) and membrane capacitive deionisation (MCDI) with natural saline streams: A critical review, Desalination. 476 (2020) 114183. https://doi.org/10.1016/j.desal.2019.114183.

[19] T. Hoshino, Innovative lithium recovery technique from seawater by using world-first dialysis with a lithium ionic superconductor, Desalination. 359 (2015) 59–63. https://doi.org/10.1016/j.desal.2014.12.018.

[20] L. Xing, J. Song, Z. Li, J. Liu, T. Huang, P. Dou, Y. Chen, X.M. Li, T. He, Solvent stable nanoporous poly (ethylene-co-vinyl alcohol) barrier membranes for liquid-liquid extraction of lithium from a salt lake brine, J. Membr. Sci. 520 (2016) 596–606. https://doi.org/10.1016/j.memsci.2016.08.027.

[21] H.J. Cassady, E.C. Cimino, M. Kumar, M.A. Hickner, Specific ion effects on the permselectivity of sulfonated poly(ether sulfone) cation exchange membranes, J. Membr. Sci. 508 (2016) 146–152. https://doi.org/10.1016/j.memsci.2016.02.048.

[22] F. Sheng, N.U. Afsar, Y. Zhu, L. Ge, T. Xu, PVA-based mixed matrix membranes comprising ZSM-5 for cations separation, Membranes (Basel). 10 (2020) 1–16. https://doi.org/10.3390/membranes10060114.

[23] N.U. Afsar, W. Ji, B. Wu, M.A. Shehzad, L. Ge, T. Xu, SPPO-based cation exchange membranes with a positively charged layer for cation fractionation, Desalination. 472 (2019) 114145. https://doi.org/10.1016/j.desal.2019.114145.

[24] N. U. Afsar, X. Ge, Z. Zhao, A. Hussain, Y. He, L. Ge, T. Xu, Zwitterion membranes for selective cation separation via electrodialysis, Sep. Purif. Technol. 254 (2021). https://doi.org/10.1016/j.seppur.2020.117619.

[25] Y. Guo, Y. Ying, Y. Mao, X. Peng, B. Chen, Polystyrene sulfonate threaded through a metal–organic framework membrane for fast and selective lithium-ion separation, Angew. Chemie - Int. Ed. 55 (2016) 15120–15124. https://doi.org/10.1002/anie.201607329.

[26] J. Zhang, X. Cui, F. Yang, L. Qu, F. Du, H. Zhang, J. Wang, Hybrid cation exchange membranes with lithium ion-sieves for highly enhanced li+ permeation and permselectivity, Macromol. Mater. Eng. 304 (2019) 1–11. https://doi.org/10.1002/mame.201800567.

[27] P.P. Sharma, V. Yadav, A. Rajput, H. Gupta, H. Saravaia, V. Kulshrestha, Sulfonated poly (ether ether ketone) composite cation exchange membrane for selective recovery of lithium by electrodialysis, Desalination. 496 (2020) 114755. https://doi.org/10.1016/j.desal.2020.114755.

[28] B. Swain, Recovery and recycling of lithium: a review, Sep. Purif. Technol. 172 (2017) 388–403. https://doi.org/10.1016/j.seppur.2016.08.031.

[29] X. Xu, Y. Chen, P. Wan, K. Gasem, K. Wang, T. He, H. Adidharma, M. Fan, Extraction of lithium with functionalized lithium ion-sieves, Prog. Mater. Sci. 84 (2016) 276–313. https://doi.org/10.1016/j.pmatsci.2016.09.004.

[30] J. Wang, Y. Liu, H. Zhang, Y. Li, H. Bai, W. Wu, Z. Li, X. Zhang, Embedding sulfonated lithium ion-sieves into polyelectrolyte membrane to construct efficient proton conduction pathways, J. Membr. Sci. 501 (2016) 109–122. https://doi.org/10.1016/j.memsci.2015.12.008.

[31] H.J. Hong, I.S. Park, T. Ryu, J. Ryu, B.G. Kim, K.S. Chung, Granulation of Li1.33Mn1.67O4 (LMO) through the use of cross-linked chitosan for the effective recovery of Li+ from seawater, Chem. Eng. J. 234 (2013) 16–22. https://doi.org/10.1016/j.cej.2013.08.060.

[32] T. Ryu, D.H. Lee, J.C. Ryu, J. Shin, K.S. Chung, Y.H. Kim, A lithium selective adsorption composite by coating adsorbent on PVC plate using epoxy-silica hybrid binder, Hydrometallurgy. 183 (2019) 118–124. https://doi.org/10.1016/j.hydromet.2018.11.011.

[33] K.S. Chung, J.C. Lee, W.K. Kim, S.B. Kim, K.Y. Cho, Inorganic adsorbent containing polymeric membrane reservoir for the recovery of lithium from seawater, J. Membr. Sci. 325 (2008) 503–508. https://doi.org/10.1016/j.memsci.2008.09.041.

[34] K.N. Jacob, S.S. Kumar, A. Thanigaivelan, M. Tarun, D. Mohan, Sulfonated polyethersulfone-based membranes for metal ion removal via a hybrid process, J. Mater. Sci. 49 (2014) 114–122. https://doi.org/10.1007/s10853-013-7682-1.

[35] A. Noshay, L.M. Robeson, Sulfonated polysulfone, J. Appl. Polym. Sci. 20 (1976) 1885–1903. https://doi.org/10.1002/app.1976.070200717.

[36] D. Lu, H. Zou, R. Guan, H. Dai, L. Lu, Sulfonation of polyethersulfone by chlorosulfonic acid, Polym. Bull. 54 (2005) 21–28. https://doi.org/10.1007/s00289-005-0361-x.

[37] R. Guan, H. Dai, C. Li, J. Liu, J. Xu, Effect of casting solvent on the morphology and performance of sulfonated polyethersulfone membranes, J. Membr. Sci. 277 (2006) 148–156. https://doi.org/10.1016/j.memsci.2005.10.025.

[38] W.H. Bragg, The reflection of X-rays by crystals [3], Nature. 91 (1913) 477. https://doi.org/10.1038/091477b0.

[39] F. Wang, M. Hickner, Y.S. Kim, T.A. Zawodzinski, J.E. McGrath, Direct polymerization of sulfonated poly(arylene ether sulfone) random (statistical) copolymers: Candidates for new proton

exchange membranes, J. Membr. Sci. 197 (2002) 231–242. https://doi.org/10.1016/S0376-7388(01)00620-2.

[40] T.D. Gierke, G.E. Munn, F.C. Wilson, Morphology in nafion perfluorinated membrane products, as determined by wide- and small-angle X-ray studies, J. Polym. Sci. Part A-2, Polym. Phys. 19 (1981) 1687–1704. https://doi.org/10.1002/pol.1981.180191103.

[41] K. Coenen, F. Gallucci, B. Mezari, E. Hensen, M. van Sint Annaland, An in-situ IR study on the adsorption of CO2 and H2O on hydrotalcites, J. CO2 Util. 24 (2018) 228–239. https://doi.org/10.1016/j.jcou.2018.01.008.

[42] M. Zheng, H. Zhang, X. Gong, R. Xu, Y. Xiao, H. Dong, X. Liu, Y. Liu, A simple additive-free approach for the synthesis of uniform manganese monoxide nanorods with large specific surface area, Nanoscale Res. Lett. 8 (2013) 1–7. https://doi.org/10.1186/1556-276X-8-166.

[43] A. Kumar, S. Logapperumal, R. Sharma, M.K. Das, K.K. Kar, Li-ion transport, structural and thermal studies on lithium triflate and barium titanate incorporated poly(vinylidene fluoride-co-hexafluoropropene) based polymer electrolyte, Solid State Ionics. 289 (2016) 150–158. https://doi.org/10.1016/j.ssi.2016.03.008.

[44] N.B. Sahli, A.M.M. Bin Ali, Effect of lithium triflate salt concentration in methyl cellulose-based solid polymer electrolytes, in: CHUSER 2012 - 2012 IEEE Colloq. Humanit. Sci. Eng. Res., 2012: pp. 739–742. https://doi.org/10.1109/CHUSER.2012.6504410.

[45] W.Y. Chuang, T.H. Young, D.M. Wang, R.L. Luo, Y.M. Sun, Swelling behavior of hydrophobic polymers in water/ethanol mixtures, Polymer (Guildf). 41 (2000) 8339–8347. https://doi.org/10.1016/S0032-3861(00)00176-2.

[46] R.M. Huertas, C.M. Doherty, A.J. Hill, A.E. Lozano, J. de Abajo, J.G. de la Campa, E.M. Maya, Preparation and gas separation properties of partially pyrolyzed membranes (PPMs) derived from copolyimides containing polyethylene oxide side chains, J. Membr. Sci. 409–410 (2012) 200–211. https://doi.org/10.1016/j.memsci.2012.03.057.

[47] J. Chen, Q. Guo, Z. Zhao, X. Wang, C. Duan, Structures and mechanical properties of PEEK/PEI/PES plastics alloys blent by extrusion molding used for cable insulating jacketing, Procedia Eng. 36 (2012) 96–104. https://doi.org/10.1016/j.proeng.2012.03.016.

[48] M. Pirali-Hamedani, S. Mehdipour-Ataei, Effect of sulfonation degree on molecular weight, thermal stability, and proton conductivity of poly(arylene ether sulfone)s membrane, Des. Monomers Polym. 20 (2017) 54–65. https://doi.org/10.1080/15685551.2016.1231035.

[49] Y. Gao, G.P. Robertson, M.D. Guiver, X. Jian, Synthesis and characterization of sulfonated poly(phthalazinone ether ketone) for proton exchange membrane materials, J. Polym. Sci. Part A Polym. Chem. 41 (2003) 497–507. https://doi.org/10.1002/pola.10601.

[50] T. Brás, D. Rosa, A.C. Gonçalves, A.C. Gomes, V.D. Alves, J.G. Crespo, M.F. Duarte, L.A. Neves, Development of bioactive films based on chitosan and Cynara cardunculus leaves extracts for wound dressings, Int. J. Biol. Macromol. 163 (2020) 1707–1718. https://doi.org/10.1016/j.ijbiomac.2020.09.109.

[51] T. Crizel, A. Rios, V.D. Alves, N. Bandarra, M. Moldão-Martins, S.H. Flôres, Biodegradable films based on gelatin and papaya peel microparticles with antioxidant properties, Food Bioprocess Technol. 11 (2018) 536–550. https://doi.org/10.1007/s11947-017-2030-0.

Abbreviations

CEM	Cation exchange membrane
CAS	Chlorosulfonic acid
DS	Degree of sulfonation
DSC	Differential scanning calorimetry
DMF	Dimethylformamide
FT-IR	Fourier transform infrared spectroscopy
HMO	$H_{1.33}Mn_{1.67}O_4$ (Hydrogen manganese oxide)
^{1}H-NMR	Nuclear magnetic resonance of proton
ICP-AES	Inductively coupled-plasma atomic emission spectroscopy

LMO	$Li_{1.33}Mn_{1.67}O_4$ (Lithium manganese oxide)
LIS	Lithium ion sieve
LSV	Linear sweep voltammetry
MOF	Metal organic framework
PES	Polyethersulfone
PSS-Na	Sodium salt of polystyrene sulfonate
SEM	Scanning electron microscopy
SPES	Sulfonated polyethersulfone
TGA	Thermogravimetric analysis
TS	Tensile strength
XRD	X-ray diffraction
WC	Water content